

COMPARISON OF ACOUSTIC AND ELASTIC FWI FOR COMPLEX SALT ENVIRONMENTS

N. Thiel and T. Bohlen

email: *niklas.thiel@kit.edu*

keywords: *elastic FWI, salt, streamer, wavefield separation, field data*

ABSTRACT

We compare applications of acoustic and elastic 2D full-waveform inversions (FWI) to marine field data that were acquired with a dual-sensor streamer offshore West Africa. For the given complex salt environment below the acquisition profile, the acoustic FWI fails to find a model that explains the field data. The elastic FWI produces a reasonable model that represents the main characteristics of the field data.

We show that converted P- to S-waves at the rough top of salt interface are quite pronounced and influence the amplitudes of P-P reflected waves considerably. For this reason, the field data cannot be explained in the acoustic approximation.

INTRODUCTION

Hydrocarbons, at least presently, are the most used energy source in the world. Energy companies are constantly looking for new reservoirs but the discovery of new hydrocarbons becomes increasingly challenging (Leveille et al., 2011). Most of the shallow reservoirs are already in production or empty. In the past, salt basins proved to be successful sites for the search. The migrated oil and gas is trapped at the bottom of salt layers or at the flanks of salt domes. The Gulf of Mexico (GoM) is probably the most well known site. But also other areas such as offshore South-East America or West Africa become more and more interesting (Leveille et al., 2011). Brognon and Verrier (1966) had already reported about the oil occurrence in the complex geology offshore Angola, West Africa. In this region the field data set used in this work was acquired.

Classical imaging techniques such as, for example, Kirchhoff migration often have problems picturing the salt body (e.g., Ravaut et al., 2008). The reason for this is the complex shape of most salt bodies and salt layers, resulting from movements of the overburden in millions of years. The salt was deposited millions of years ago and other sediments deposited on top. The lower density of salt in comparison to the surrounding sediments and the high load of the above sediments allowed the salt to move upwards and formed canopies. This leads to a strong topography of the salt structure. In addition to the shape, the allochthonous salt layers often contain trapped sediments and have a rugose surface (Leveille et al., 2011). The intricate shapes and surfaces of salt bodies result in complex wave propagation. Regions of poor illumination are often present. Additionally, the energy coming up from subsalt regions is weak due to high reflection coefficients at the sediment-salt interface.

As possible geological misinterpretations are very expensive, reliable processing and imaging methods must be developed. For smaller salt bodies methods like undershooting and the use of longer offsets lead to good results (e.g. Corcoran et al., 2007). However, for integrated salt layers even these techniques are not applicable. A promising solution for the problem of imaging the salt environment is the application of full-waveform inversion (FWI). Unlike conventional techniques the entire waveform is used in the FWI approach. Synthetic data are modelled by using a starting model of the subsurface beneath the acquisition profile. The synthetic data are then compared to the field data. In order to match the synthetic data to the

field data the starting model is updated iteratively. By using the full information of the acquired wavefield the FWI process can improve the model and depth image considerably.

In this work we image a salt layer with a complex structure using field data. We explain why elastic FWI is necessary for a successful inversion of the field data and why the acoustic approximation is insufficient.

FIELD DATA AND MODEL

The used field data set is part of a 2D marine line from offshore West Africa, provided by PGS. The data were shot over a continuous salt layer and recorded by a dual-sensor towed streamer. The delivered data set had already been wavefield-separated. In addition to the data, PGS provided us with a starting model derived from migration velocity analysis. This model was used as the starting model in FWI.

The raw data set is a profile of 265 km length and a shot interval of 50 m. For test purpose, we limited the model to 20 km profile length and used only every 10th shot. This leads to 19 shots with a shot spacing of 500 m. The streamer was towed in 20 m depth and the first receiver has a distance of 100 m to the source. With 804 traces per shot, the maximum offset is more than 10 km. As the water is more than 2 km deep and the salt in parts more than 6 km thick, we use 12 s of recording time.

Due to the use of a two-dimensional inversion code we performed a 3D-2D transformation on the field data using the software *lisousi* (Forbriger et al., 2014). Each trace is convolved with $1/\sqrt{t}$ and multiplied by $v\sqrt{t}$ with t being traveltimes and v being velocity. Also, a resampling to 1 ms for the acoustic case and 0.6 ms for the elastic case was performed to avoid instabilities.

PGS provided us with an interpreted detailed velocity model including the salt layer and a smooth background model. The model has a dimension of 20 km in x-direction and 8 km in depth direction. The grid distance was set to 12.5 m in the acoustic case and 6.25 m for the elastic inversion. A larger sampling interval in space was not possible as dispersion effects have to be avoided. For the total model this results in about 1 million grid points and 4.1 million grid points, respectively.

INVERSION STRATEGY

In this work we use the two-dimensional FWI code IFOS2D (e.g. Köhn, 2011). The code uses the time-domain stress-velocity finite-difference formulation on a standard staggered grid for the forward modelling as described by Bohlen (2002). The gradients are derived using the adjoint state method (Tarantola, 1984).

In order to quantify the misfit between the real and modelled data the L2-norm in its normalised version is used. It proved to be more robust for field data than the standard L2-norm (Choi and Alkhalifah, 2012). The inversion was started using a low-pass filter of 5 Hz for the data. During the inversion, the maximum frequency is increased up to 14 Hz (up to 10 Hz in the elastic case). Starting at low frequencies and increasing the frequency content stepwise avoids the occurrence of cycle skipping.

To decrease the influence of noise on the inversion result and, therefore, the occurrence of artefacts (unrealistic structures) in the inversion result, the field seismograms are muted before the first arrival. In order to make the synthetic data and field data comparable for the inversion process, using the correct source wavelet plays an important role in the forward modelling. Therefore, the source time functions for all shots are inverted from the field data before every frequency step.

We invert also for the density parameter. The starting model for density was derived by applying the Gardner relation (Gardner et al., 1974) on the v_P model.

DATA AND WAVEFIELD SNAPSHOTS

In order to study the influence of elastic properties on the wavefield, snapshots of acoustic and elastic forward-modelled wavefields are displayed in figure 2. The wavefields were propagated in the model shown in figure 3(a) and a snapshot for shot 7 was taken at $t = 4.44$ s. For better orientation, two black lines were added to the snapshots: the upper line represents the sea floor and the lower line the top of salt. To ensure comparability, all snapshots are scaled equally. The upper three plots show the divergence of the acoustically or elastically modelled wavefield. The divergence represents the P-wave part of the full wavefield. The curl of the elastic modelling is plotted in figure 2(d), representing the S-wave part. For acoustic modelling, the curl is zero. A significant curl component can only be observed in the sediments above the salt. In water, the S-wave velocity is zero, but the P-wave is converted partly into S-waves after hitting the

sea floor. Also, parts of the P-wave hitting the top of salt are converted into S-waves. A comparison of the amplitudes in the snapshots of the curl and divergent components shows that a considerable amount of the P-wave energy was converted into S-waves.

The difference plot in figure 2(c) shows the discrepancies of both divergence components of the wavefield snapshots. Since water is assumed as pure acoustic medium, the direct wave is the same in the acoustic and elastic simulation. Thus, the direct wave (first event from the left or right side at the surface in the first two plots) is not visible in the difference plot. Also, the reflection of the seafloor (second event from the left or right side at the surface in the first two plots) is hardly visible, as only little energy is converted into S-waves. Most of the differences appear in the reflection from the top of salt (TOS). In the upper two snapshots of the wavefield in figures 2, this event can be located as third event from the left or right border of the model at the water surface.

From the high amplitudes in the difference plot it can be concluded that the elastic effects in the presence of salt are considerable. But the effect does not appear as additional events. By comparing the wavefield snapshots of the divergence and curl components of the elastic forward modelling it can be observed that the main part of the converted energy is trapped in the sediment layer between the sea floor and the TOS, or transmitted into the salt layer. Therefore, the main differences in the seismograms are the change of relative amplitudes of the events. This effect makes it difficult for the acoustic inversion to adapt the waveforms. Despite the use of normalised seismograms, the relative difference in amplitude between the events is still present.

FIELD DATA INVERSION RESULTS

Acoustic

The starting model of the v_P -component of the acoustic FWI is shown in figure 3(a). The source positions are indicated by red stars. The streamer is located on the left side of the shots and moves with the shots from left to right.

The inversion results are plotted in figure 3. The inversion was able to reduce the data misfit by 20 % in 98 iterations, up to a frequency of 14 Hz. From the development of the misfit curve it can be noticed that the misfit was clearly reduced during the first frequency stage and the minimum misfit is already reached after the change to the second frequency stage. But after including frequencies up to 6 Hz, the misfit starts to increase. Then, after changing to 7 Hz, the misfit value drops again. This unusual behaviour indicates that the inversion is unable to find an update reducing the data misfit. The reason for this can be explained by an attempt of the inversion trying to explain elastic data with acoustic modelling. Therefore, the inversion results need to be interpreted carefully, as the models can include artefacts.

The inversion results of the v_P model and the density model are plotted in figure 3(b)-3(c). The inversion of the v_P parameter updated only long-wavelength structures in the sediment layer above the salt. Above the valley in the middle of the TOS, a lower velocity valley is visible and higher-velocity layers below. The density model shows more detailed structures in the sediment layer. On the right side of the valley, a high-density layer was included above the salt. Above the valley of the TOS, two well defined high-density layers were added. Layered structures are also visible on the left side of the valley. The updates seem to be blocky, which is interpreted as a result of artefacts. Also, the contrasts between the low- and high-density structures are very high with partly almost $100 \frac{\text{kg}}{\text{m}^3}$ difference within a few hundred metres. This can be explained by the acoustic approximation and the attempt of the inversion to fit amplitudes in the elastic data. As the high-velocity/density layers are continuous throughout the model, though, they seem reasonable and they are not interpreted as artefacts.

In order to evaluate the results, the data fit is plotted in figure 3(e). Some of the main events could be fitted, but still most events could not, neither in phase nor in amplitude. The same can be seen by comparing the field data and the inverted shot gather in figure 3(g) and 3(h). Only the main events were fitted. A comparison of the results of the STF inversion (figure 3(f)) shows also large differences. Especially in the middle, the STF inversion results differ strongly from each other. These differences indicate insufficiencies in the starting model.

The resulting v_P parameter of the acoustic inversion shows only long-wavelength structures. The density results show well defined high-density layers above the top of salt, interspersed with small-scale arte-

facts. In the results it is difficult to distinguish between artefacts and structures.

Elastic

The results of the elastic inversion after 89 iterations (up to 10 Hz) of the v_P and density component are shown in figure 4(b)-4(c). The v_S result is not shown as it contains almost no updates. The reason for this is that almost no converted energy is back-propagating into the water (see previous section). Again, the density update is most detailed in the sediments area above the salt. Various high-density layers were added to the starting model, following roughly the topography of the salt. Some small-scale horizontal artefacts are visible, caused by the acquisition geometry. The application of a horizontal filtering of the gradients had no positive effect on the result. Therefore, we decided not to use the filter.

After all iterations, the inversion was able to reduce the misfit by almost 60 % (figure 4(d)). In order to evaluate the quality of the result, the data fit of selected models, the STF inversion results and the comparison of the field and inverted data are plotted (figure 4(e)- 4(h)). For the data fit, three traces are plotted, for a near, middle and far offset, respectively. In black, the true data filtered to the corresponding frequency are plotted, overlain by the inverted traces. The main events could be fitted in phase and amplitude. Also, the STF inversion results show a consistent behaviour for all shots. Only the 10th shot seems to be shifted down by about 0.05 s. The synthetic data could be fitted very well to the field data (figure 4(g) and 4(h)). All main phases match in phase as well as in amplitude.

All in all it can be concluded that the elastic inversion using the PGS model as starting model was successful and the results are reasonable. The density update shows several continuous high-density layers. In comparison with the acoustic inversion, a considerable lower misfit was achieved and clearly more details are present in the density update.

CONCLUSIONS

This field data test shows the importance of elastic FWI. Even for high-quality marine towed-streamer data, where the acoustic approximation of FWI is commonly used, the elastic FWI shows considerable advantages for complex salt environments. The inversion results look much more detailed and reasonable. The monitoring parameters confirm that the detailed result does not contain many artefacts. The data misfit was reduced compared to acoustic FWI (indicated by the much lower values of the objective function), and the STF inversion results look far more homogeneous among themselves.

Based on the results of this study, we recommend to use elastic FWI for marine data in complex salt environment, despite the higher computational costs.

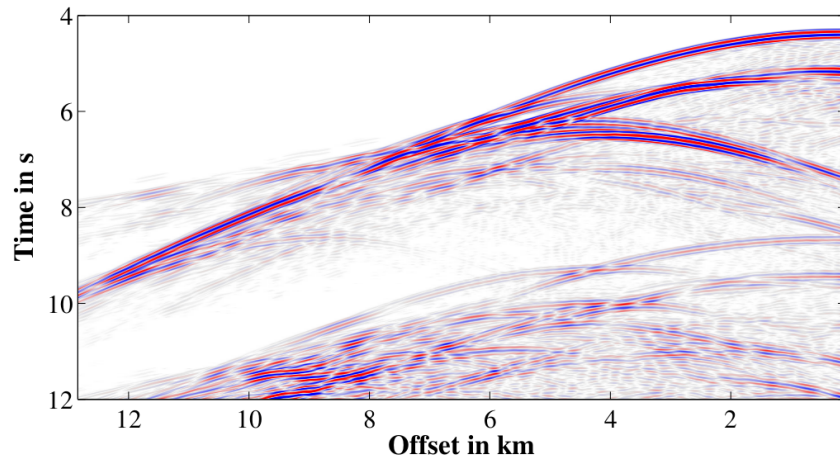
ACKNOWLEDGEMENTS

We thank PGS for providing the data set and model. This work was kindly supported by the sponsors of the *Wave Inversion Technology (WIT) Consortium*. We gratefully acknowledge the computing time granted on the supercomputer ForHLR II at KIT.

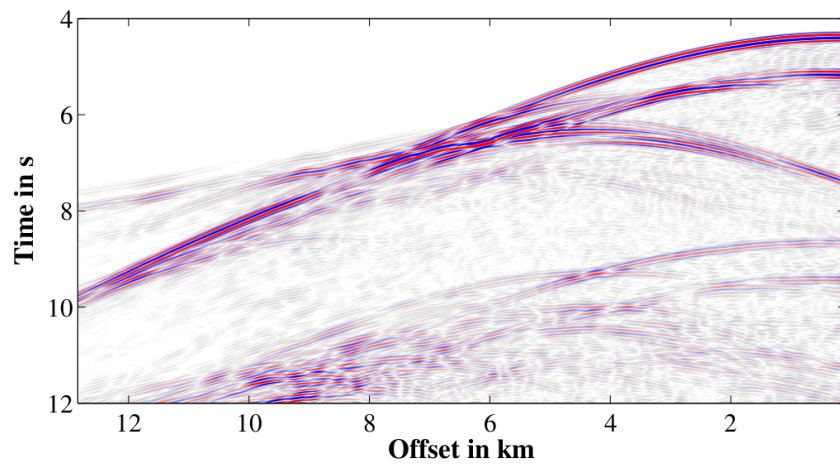
REFERENCES

- Bohlen, T. (2002). Parallel 3-D viscoelastic finite difference seismic modelling. *Computers & Geosciences*, 28(8):887–899.
- Brognon, G. P. and Verrier, G. R. (1966). Oil and geology in Cuanza Basin of Angola. *AAPG Bulletin*, 50(1):108–158.
- Choi, Y. and Alkhalifah, T. (2012). Application of multi-source waveform inversion to marine streamer data using the global correlation norm. *Geophysical Prospecting*, 60:748–758.
- Corcoran, C., Perkins, C., Lee, D., Cattermole, P., Cook, R., and Moldoveanu, N. (2007). A wide-azimuth streamer acquisition pilot project in the Gulf of Mexico. *The Leading Edge*, 26(4):460–468.
- Forbriger, T., Groos, L., and Schäfer, M. (2014). Line-source simulation for shallow-seismic data. Part 1: Theoretical background. *Geophysical Journal International*, 198(3):1387–1404.

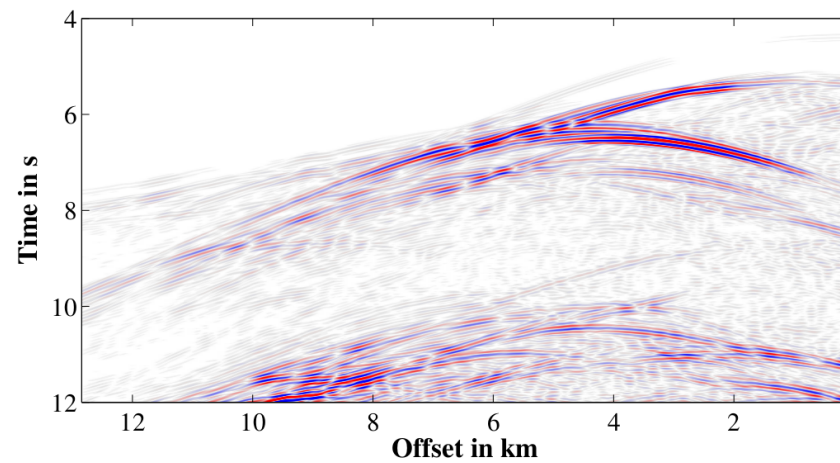
- Gardner, G. H. F., Gardner, L. W., and Gregory, A. R. (1974). Formation basics for velocity and density - the traps diagnostic stratigraphic. *Geophysics*, 39(6):770–780.
- Köhn, D. (2011). *Time Domain 2D Elastic Full Waveform Tomography*. PhD thesis, Christian-Albrechts-Universität zu Kiel.
- Leveille, J. P., Jones, I. F., Zhou, Z.-Z., Wang, B., and Liu, F. (2011). Subsalt imaging for exploration, production, and development: A review. *Geophysics*, 76(5):WB3–WB20.
- Ravaut, C., Alerini, M., Pannetier-Lescoffit, S., and Thomassen, E. (2008). Sub-salt imaging by full-waveform inversion: a parameter analysis. In *2008 SEG Annual Meeting*.
- Tarantola, A. (1984). Inversion of seismic reflection data in the acoustic approximation. *Geophysics*, 49(8):1259–1266.



(a) Acoustic modelling.

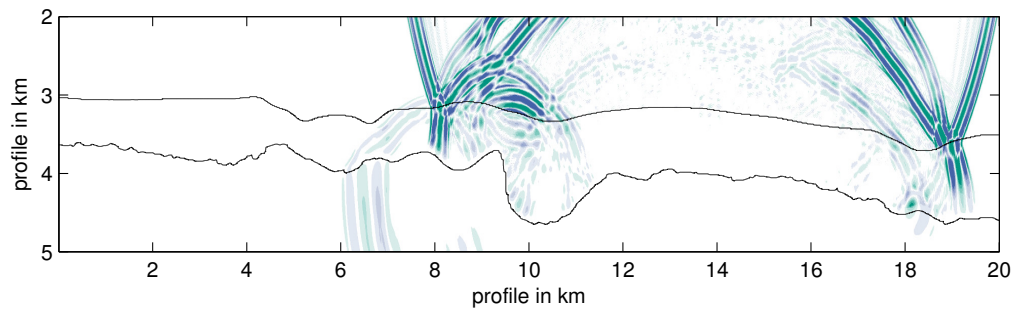


(b) Elastic modelling.

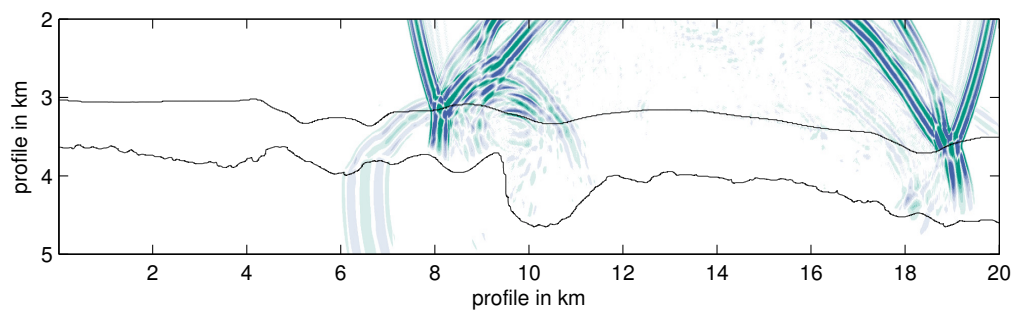


(c) Difference of the seismograms in figure 1(a) and 1(b).

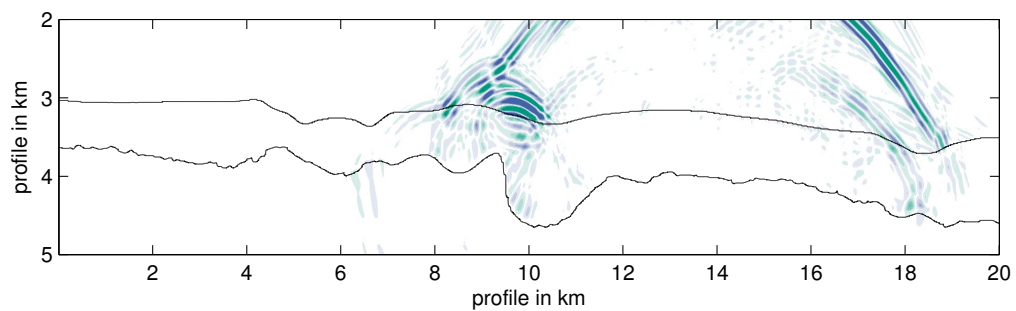
Figure 1: Comparison of acoustic and elastic forward-modelled seismograms (pressure component) in the test model shown in figure 3(a), shot 7.



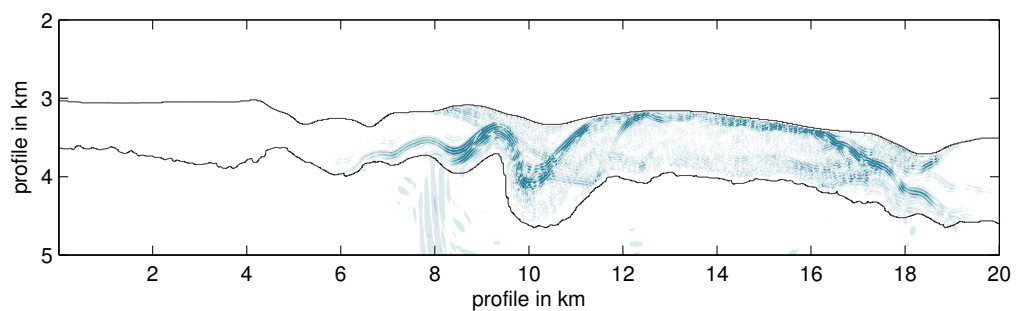
(a) Divergence component of the acoustically forward-modelled wavefield.



(b) Divergence component of the elastically forward-modelled wavefield.



(c) Difference wavefield of the divergence components shown in figure 2(a) and 2(b).



(d) Curl component of the elastic forward-modelled wavefield.

Figure 2: Comparison of acoustically and elastically forward-modelled wavefields. Snapshots of the forward-simulated wavefield in the test model shown in figure 3(a) at $t = 4.44$ s. The first contour line in black represents the sea floor, the lower contour line the top of salt. All plots are scaled equally.

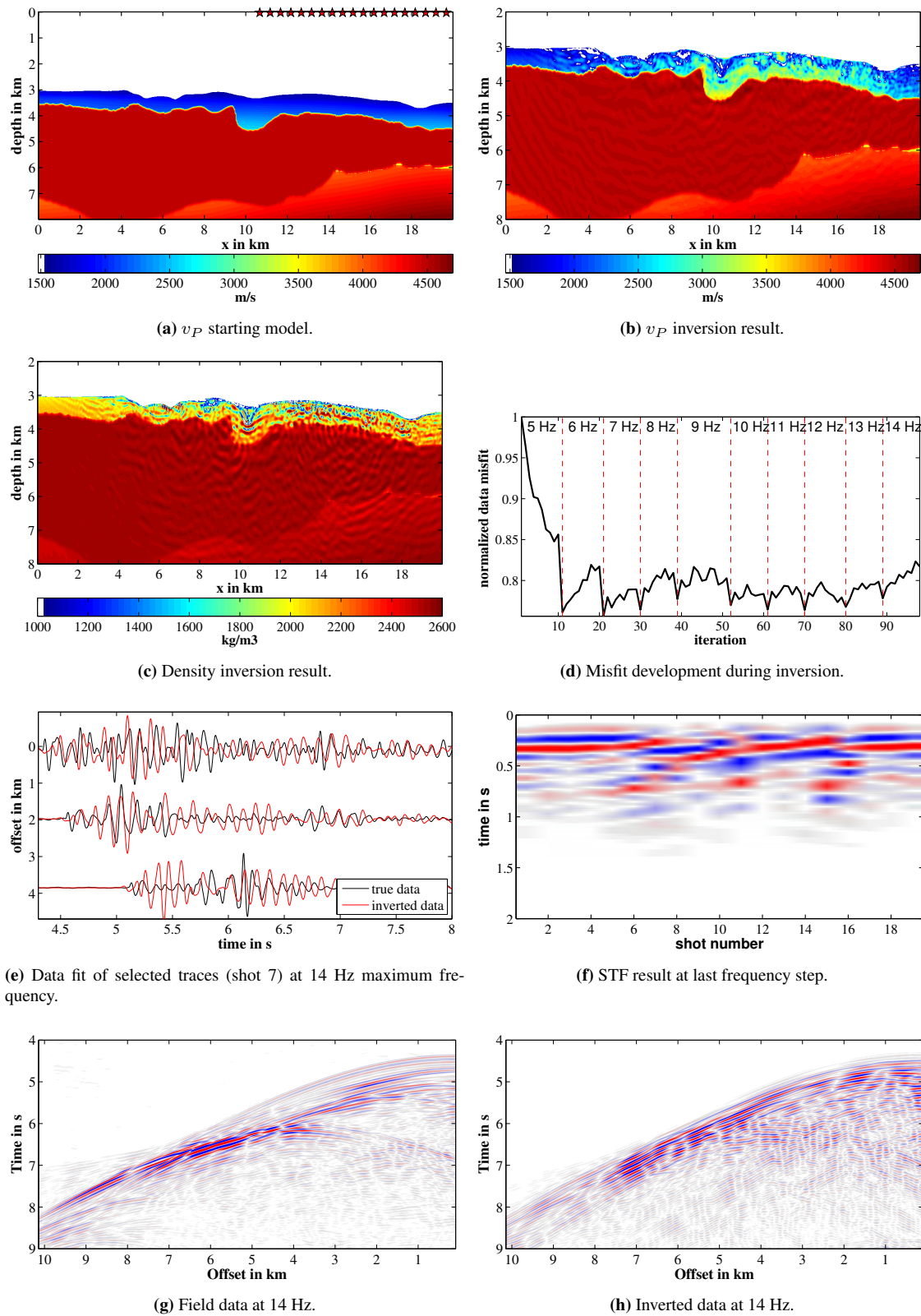


Figure 3: Inversion results of acoustic inversion after 89 iterations, using the PGS model as starting model.

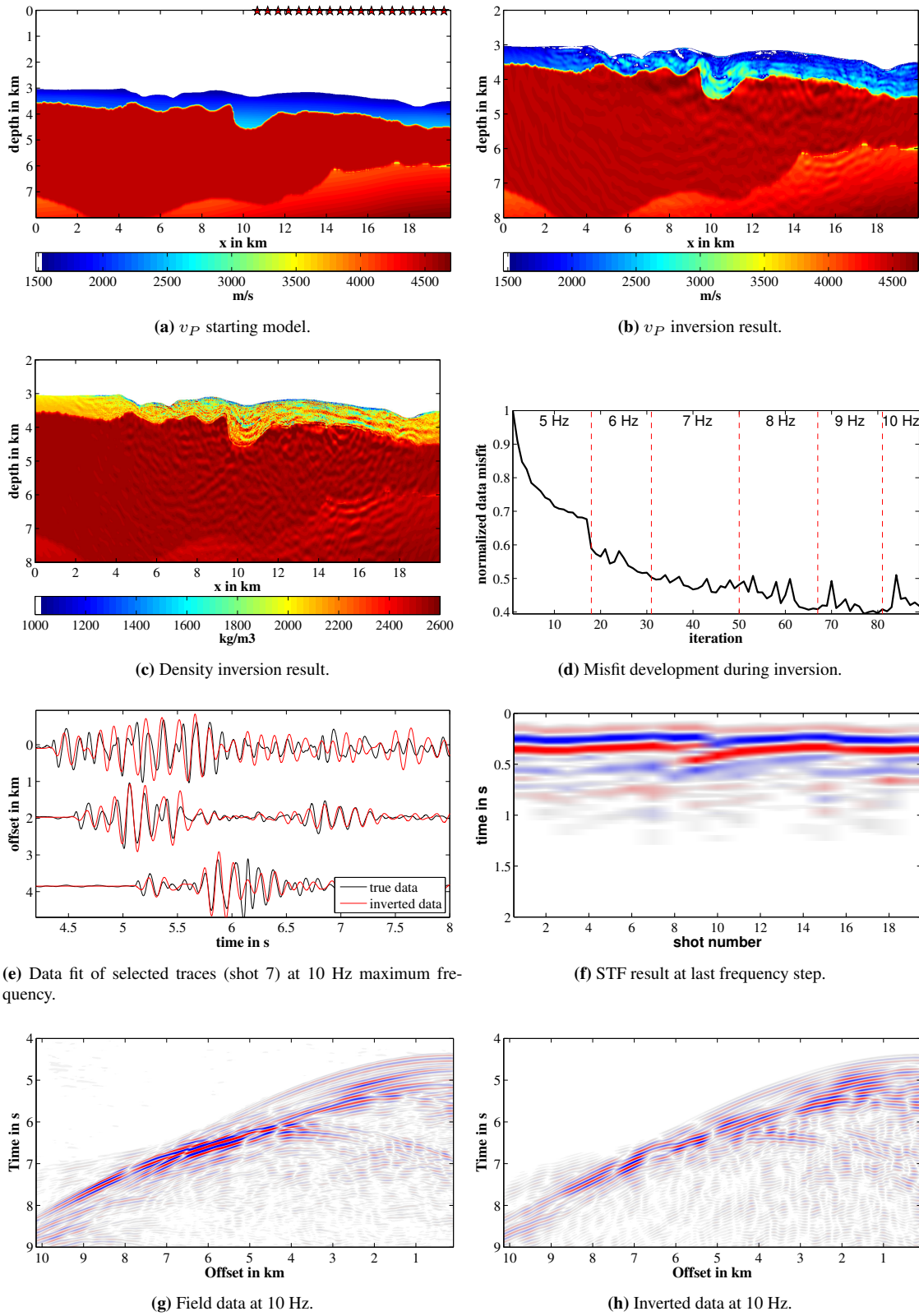


Figure 4: Inversion results of elastic inversion after 89 iterations, using the PGS model as starting model.